Journal of Inorganic Biochemistry 167 (2017) 49–59

Contents lists available at ScienceDirect

Journal of Inorganic Biochemistry

journal homepage: www.elsevier.com/locate/jinorgbio

Dimerization, redox properties and antioxidant activity of two manganese(III) complexes of difluoro- and dichloro-substituted Schiff-base ligands

Claudia Palopoli [a], Guillermo Gómez [a], Ana Foi [b], Fabio Doctorovich [b], Sonia Mallet-Ladeira [c], Christelle Hureau [d], Sandra Signorella [a,*]

[a] IQUIR (Instituto de Química Rosario), Consejo Nacional de Investigaciones Científicas y Técnicas (CONICET), Facultad de Ciencias Bioquímicas y Farmacéuticas, Universidad Nacional de Rosario, Suipacha 531, S2002LRK Rosario, Argentina
[b] Departamento de Química Inorgánica, Analítica y Química Física/INQUIMAE-CONICET, Facultad de Ciencias Exactas y Naturales, Universidad de Buenos Aires, Ciudad Universitaria, Pabellón 2, Buenos Aires C1428EHA, Argentina
[c] Institut de Chimie de Toulouse, FR 2599, 118 Route de Narbonne, F-31062 Toulouse, France
[d] CNRS, LCC (Laboratoire de Chimie de Coordination) and UPS, INPT, LCC, Université de Toulouse, 205 route de Narbonne, F-31077 Toulouse, France

ARTICLE INFO

Article history:
Received 23 June 2016
Received in revised form 8 November 2016
Accepted 16 November 2016
Available online 18 November 2016

Keywords:
Mn catalysts
Structure
SOD/CAT activity
Dimerization
Kinetics

ABSTRACT

Two mononuclear Mn^{III} complexes $[Mn(3,5\text{-}F_2salpn)(H_2O)_2][B(C_6H_5)_4]\cdot 2H_2O$ (**1**·$2H_2O$) and $[Mn(3,5\text{-}Cl_2salpn)(OAc)(H_2O)]\cdot H_2O$ (**2**·H_2O), where H_2salpn = 1,3-bis(salicylidenamino)propane, have been prepared and characterized. The crystal structure of **1**·H_2O shows that this complex forms μ-aqua dimers with a short Mn···Mn distance of 4.93 Å. Under anaerobic conditions, the two complexes are stable in solution and possess *trans*-diaxial symmetry with the tetradentate Schiff base ligand symmetrically arranged in the equatorial plane. When left in air, these complexes slowly dimerize to yield high-valent $[Mn^{IV}_2(3,5\text{-}X_2\text{-}salpn)_2(\mu\text{-}O)_2]$ in which each X_2-salpn ligand wraps the two Mn ions. This process is favored in basic medium where the deprotonation of the bound water molecule is concomitant with air oxidation. The two complexes catalyze the dismutation of superoxide (superoxide dismutase (SOD) activity) and peroxide (catalase (CAT) activity) in basic medium. The phenyl-ring substituents play an important role on the CAT reaction but have little effect on SOD activity. Kinetics and spectroscopic results indicate that **1** and **2** catalyze H_2O_2 disproportionation through a cycle involving Mn^{III}_2 and Mn^{IV}_2 dimers, unlike related complexes with a more rigid and smaller chelate ring, which employ Mn^{III}/Mn^{V}═O monomers.

1. Introduction

Reactive oxygen species (ROS) such as H_2O_2 and $O_2^{\bullet -}$, cause cell injury and have been implicated in a number of neurodegenerative diseases [1,2]. Manganese catalases (MnCAT) and superoxide dismutases (MnSOD) catalyze disproportionation of intracellular H_2O_2 and $O_2^{\bullet -}$ efficiently and constitute the main line of defense for controlling these toxic oxygen metabolites in a number of organisms, through a mechanism involving cyclic oxidation and reduction of the metal cofactor [3–5]. The active site MnSOD contains one pentacoordinate Mn ion in a N_3O_2 environment to decompose $O_2^{\bullet -}$ [5] while MnCAT catalyses the disproportionation of H_2O_2 by using a $Mn_2(\mu\text{-}O_2CR)(\mu\text{-}O/OH)$ structural unit [6]. Due to the potential use as catalytic reactive ROS scavengers for preventing oxidative stress injuries, numerous mono- and dinuclear Mn models exhibiting SOD- and CAT-like activity have been reported [7,8]. Interestingly, a number of mononuclear Mn complexes possess dual CAT/SOD activity [9–18]. These catalytic ROS scavengers would be clinically superior to stoichiometric ones [19] and should have better bioavailability than exogenously administered antioxidant enzymes [9,11]. In particular, Mn-Schiff-base complexes have proven to be efficient ROS scavengers and to protect cells from oxidative damage in several animal models [20,21]. While a number of studies have been reported for the dual SOD/CAT activity of mononuclear Mn-Schiff-base complexes, the mechanism of their CAT-like reaction remains poorly understood. Complexes of the Mn-salen (salen = 1,2-bis(salicylidenamino)ethane) family have been proposed to react through a mechanism involving mononuclear Mn^{III}/Mn^{V}═O species [9,21–24] and spectroscopic evidence for the formation of Mn^{V}═O species upon O—O bond heterolysis of a peroxo species has been reported for Mn-salophen (salophen = *N,N′*-bis(salicyliden)-1,2-phenylendiamine) [25,26] in accordance with theoretical predictions for the Mn-salen model [27,28]. However, other authors related the catalytic activity of complexes of the Mn-salen and/or Mn-salpn (salpn = 1,3-bis(salicylidenamino)propane) families to their ability to form dimers [13,29,30]. This divergence could imply that, depending on the phenol-ring substituent and geometry,

* Corresponding author.
E-mail address: signorella@iquir-conicet.gov.ar (S. Signorella).

http://dx.doi.org/10.1016/j.jinorgbio.2016.11.019
0162-0134/

these Mn-Schiff-base complexes may react via a high-valent Mn-oxo form, or through a mechanism involving dimeric Mn_2 species as do the enzyme and other mononuclear Mn complexes [31–35]. The kinetic study of the antioxidant activity of new examples of this type of Mn complexes can help to unravel some clues of their mode of action. With this aim, we report here the synthesis, characterization, properties and kinetic studies of SOD/CAT activity of $[Mn(3,5\text{-}F_2salpn)(H_2O)_2][B(C_6H_5)_4]\cdot 2H_2O$ (**1**·2H_2O) and $[Mn(3,5\text{-}Cl_2salpn)(OAc)(H_2O)]\cdot H_2O$ (**2**·H_2O) (Scheme 1), and compare their catalytic activity with that of other Mn-Schiff-base catalysts.

2. Experimental section

2.1. Materials

All reagents or AR chemicals were used as purchased. Solvents were purified by standard methods. The concentration of H_2O_2 stock solution was determined by iodometric titration.

2.2. Synthesis of ligands

2.2.1. Synthesis of 1,3-bis(3,5-difluorosalicylidenamino)propane (3,5-F_2salpn)

A mixture of 3,5-difluorosalicylaldehyde (500.3 mg, 3.16 mmol) and 1,3-diaminopropane (117.5 mg, 1.58 mmol) in ethanol (6.5 mL) was stirred at reflux for 1 h. The reaction mixture was cooled to room temperature and 3,5-F_2salpn precipitated as yellow needles, filtered off and dried under vacuum. Yield: 399.9 mg (1.13 mmol, 72%). Melting point: 118–119 °C. ^{1}H NMR (CCl_3D) δ: 8.34 (s, 2 H, N═C<u>H</u>—), 6.94 (*ddd*, 2 H, H4, $^4J_{HH}$ = 3.1; $^3J_{HF}$ = 8.2 and 10.8 Hz), 6.79 (*ddd*, 2 H, H6, $^4J_{HH}$ = 3.1; $^3J_{HF}$ = 8.2; $^5J_{HF}$ = 1.8 Hz), 3.77 (t, 4H, N—C<u>H</u>$_2$—CH_2—, J = 6.75 Hz), 2.16 (q, 2H, —CH_2—C<u>H</u>$_2$—CH_2—, J = 6.75 Hz). ^{19}F NMR (CCl_3D) δ (vs Cl_3CF): −133.24 (d, F3, J = 10.8), −123.36 (t, F5, J = 8.2). ^{19}F NMR (D_4-methanol) δ (vs Cl_3CF): −135.31 (d, F3, J = 10.8), −127.19 (t, F5, J = 8.2). UV–visible (UV–vis) λ_{max} nm (ε M^{-1} cm^{-1}) in DMF: 323 (6660), 419 (1500); in 1.75 × 10^{-4} M NaOH (DMF): 327 (5050), 398 (7750). Significant IR bands (KBr, ν cm^{-1}): ν_{OH} 3.434, ν_{CH} 3088, 2953, 2877, $\nu_{C=N}$ 1643, $\nu_{Ar\ ring\ stretch}$ 1604, 1488, $\nu_{Ar-OH\ bend}$ 1331, $\nu_{Ar-C-H\ out-of-plane}$ 851, 804.

2.2.2. Synthesis of 1,3-bis(3,5-dichlorosalicylidenamino)propane (3,5-Cl_2salpn)

This ligand was prepared through a procedure slightly modified from previously reported [36]. A mixture of 3,5-chlorosalicylaldehyde (500.4 mg, 2.62 mmol) with 1,3-diaminopropane (97.4 mg, 1.3 mmol) in ethanol (15 mL) was stirred at reflux for 2 h. The reaction mixture was cooled to room temperature and 3,5-Cl_2salpn precipitated as a pure yellow solid. Yield: 475 mg (1.13 mmol, 86%). Melting point: 172–173 °C. ^{1}H RMN ($CDCl_3$) δ: 8.31 (s, 2 H, N = C<u>H</u>—), 7.42 (d, 2 H, H4, J = 2.64 Hz), 7.16 (d, 2 H, H6, J = 2.64 Hz), 3.78 (t, 4 H, N—C<u>H</u>$_2$—CH_2, J = 6.75 Hz), 2.15 (q, 2 H, —CH_2—C<u>H</u>$_2$—CH_2—, J = 6.75 Hz). UV–visible (UV–vis) λ_{max} nm (ε M^{-1} cm^{-1}) in MeOH: 234 (43150), 280 (17200), 334 (7740), 422 (11300); in DMF 333 (6340), 427 (6380); in 5.0 × 10^{-4} M Bu_4NOH (DMF): 327 (4760), 421 (11500). Significant IR bands (KBr, ν cm^{-1}): ν_{OH} 3443, ν_{CH} 3071, 2948, 2859, $\nu_{C=N}$ 1631, $\nu_{Ar\ ring\ stretch}$ 1601, 1460, $\nu_{Ar-OH\ bend}$ 1356, $\nu_{Ar-C-H\ out-of-plane}$ 871, 733.

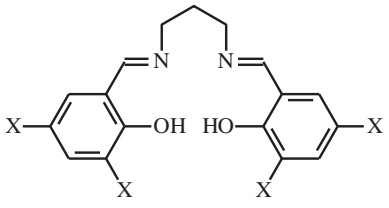

Scheme 1. Ligands used in this work: 3,5-F_2salpn: X = F; 3,5-Cl_2salpn: X = Cl.

2.3. Synthesis of complexes

2.3.1. Synthesis of $[Mn(3,5\text{-}F_2salpn)(H_2O)_2][B(C_6H_5)_4]\cdot 2H_2O$ (**1**·2H_2O)

A methanol solution (2 mL) of $Mn(OAc)_2\cdot 4H_2O$ (34.6 mg, 0.14 mmol) was slowly added to a solution of 3,5-F_2salpn (50.2 mg, 0.14 mmol) in methanol (3.5 mL) and the brownish mixture was left to stir for 24 h. Then, a methanol solution of $NaBPh_4$ (48 mg, 0.14 mmol in 0.5 mL) was added and a brown precipitate formed immediately. The solid was collected by filtration, washed with hexane and dried under vacuum. Yield: 69 mg (0.09 mmol, 62%). Anal. calcd. for $BC_{41}F_4H_{40}MnN_2O_6$: C 61.7; H 5.0; Mn 6.9, N 3.5%; found: C 61.5; H 4.9; Mn 6.8, N 3.8%. Molar conductivity (methanol) = 55 Ω^{-1} cm^2 mol^{-1}. ESI-MS: m/z = 407.02 [**1** - BPh_4 - 2H_2O]$^+$. ^{1}H NMR (D_4-methanol) δ: 18.9 (—CH_2—, $w_{1/2}$~1000 Hz), −14.3 (H4, $w_{1/2}$ = 500 Hz). ^{19}F NMR (D_4-methanol) δ (vs Cl_3CF): −60.22 ($w_{1/2}$ = 737 Hz), −74.76 ($w_{1/2}$ = 311 Hz). UV–visible (UV–vis) λ_{max} nm (ε M^{-1} cm^{-1}) in MeOH: 265 (26240), 382 (8020), 551 (505); in DMF: 375 (9930), 500–600 (265, broad): in 1.75 × 10^{-4} M Bu_4NOH (DMF): 370 (11596), 500–600 (broad). Significant IR bands (KBr, ν cm^{-1}): ν_{OH} 3472 (broad), ν_{CH} 3050, 2999, 2926, $\nu_{C=N}$ 1612, ν_{Ar} 1565, 1461, $\nu_{Ar-C-H\ out-of-plane}$ 857, 830, 738 (BPh_4), 708 (BPh_4), 612 (BPh_4). Single crystals of **1**·H_2O suitable for X-ray diffraction were obtained by crystallization from methanol upon standing for several days.

2.3.2. Synthesis of $[Mn(3,5\text{-}Cl_2salpn)(OAc)(H_2O)]\cdot H_2O$ (**2**·H_2O)

A mixture of 3,5-Cl_2salpn (251.2 mg, 0.60 mmol) and $Mn(OAc)_2\cdot 4H_2O$ (151.9 mg, 0.62 mmol) in methanol (9.5 mL) was stirred at room temperature for 48 h and a solid began to form slowly. After standing for 4 days, the resulting dark green precipitate was collected by filtration, washed with hexane and dried under vacuum. Yield: 221.3 mg (0.39 mmol, 65%). Anal. calcd. for $C_{19}Cl_4H_{19}MnN_2O_6$: C 40.2; H 3.4; Mn 9.7; N 4.9%; found: C 40.0; H 3.4; Mn 9.9, N 4.5%. Molar conductivity (methanol) = 47 Ω^{-1} cm^2 mol^{-1}. ^{1}H NMR (D_4-methanol) δ: 18.9 (—CH_2—, $w_{1/2}$ ~1000 Hz), −16.2 (H4, $w_{1/2}$ = 370 Hz). ^{1}H NMR (D_7-DMF) δ: −8.2 (H4, $w_{1/2}$ = 220 Hz). UV–vis $\lambda_{máx.}$ (ε M^{-1} cm^{-1}) in MeOH: 226 (39160), 284 (19090), 386 (7825), 559 (504); in DMF: 374 (17980), 440 (sh); in 5.0 × 10^{-4} M Bu_4NOH (DMF): 367 (14720), 505 (sh). Significant IR bands (KBr, ν cm^{-1}): ν_{OH} 3430 (broad), ν_{CH} 3083, 2929, 2860, $\nu_{C=N}$ 1615, ν_{Ar} 1589, 1438, ν_{CO2-} 1554/1389, $\nu_{Ar-C-H\ out-of-plane}$ 870, 770.

2.4. Physical and analytical measurements

Electronic spectra were recorded on a JASCO V550 spectrophotometer with thermostated cell compartments. IR spectra were recorded on a Perkin-Elmer Spectrum One FT-IR spectrophotometer. ESI-mass spectra were recorded on a Q-TRAP AB SCIEX instrument. The solutions for electrospray were prepared from solutions of the complexes or reaction mixtures and diluted with methanol to a ≈10^{-5} M concentration at a flow rate of 5 mL min^{-1}. Melting point was taken on a Fisher-Johns (Ionomex) apparatus. ^{1}H and ^{13}C NMR spectra were recorded on a Bruker AC 300 NMR spectrometer at ambient probe temperature (ca. 26 °C). Chemical shifts are referenced to Cl_3CF (^{19}F NMR) and $(CH_3)_4Si$ (^{1}H NMR) and downfield shifts are given a positive sign. Paramagnetic NMR spectra were acquired using super WEFT sequence, with acquisition time of 23 ms. For ^{19}F NMR measurements, a fluorine frequency of 282.3 MHz was used. EPR spectra were obtained on a Bruker ESP 300 E spectrometer with a microwave frequency generated with a Bruker ER 04 (9–10 GHz). Conductivity measurements were performed using a Horiba F-54 BW conductivity meter, on 1.0 mM solutions of the complexes in methanol. The electrochemical experiments were performed with a computer-controlled Princeton Applied Research

potentiostat, model VERSASTAT II, with model 270/250 Research Electrochemistry Software. Studies were carried out under Ar, in MeOH, DMF or DMSO solutions using 0.1 M Bu_4NPF_6 as a supporting electrolyte and $\approx 10^{-3}$ M of the complex. The working electrode was a Pt wire (MeOH, DMF) or a glassy carbon disk (DMSO) and the reference electrode was SCE with Pt as the auxiliary electrode. All potentials are referred to the SCE electrode. Using the described conditions, the ferrocene/ferrocenium redox couple was observed at $E_{1/2} = 409$ mV in MeOH, $E_{1/2} = 473$ mV in DMF and $E_{1/2} = 417$ mV in DMSO.

2.5. Evaluation of CAT activity

Oxygen evolution studies were carried out polarographically using a Clark-type oxygen electrode with an YSI oxygen-monitoring system (Model 5300, Yellow Springs Instruments Co., Inc.). The initial rate method was used to determine the rate constants (see ref. 37 for further details). Each rate constant reported here represents the mean value of multiple determinations that fall within ±5%. Experiments were carried out at 25 °C. Alternatively, rates were determined by volumetric measurement of the evolved O_2 from reaction mixtures. A round-bottom flask with a stopcock equipped gas delivery side tube connected to a gas-measuring burette (precision of 0.1 mL) was used. A closed vessel containing a solution of catalyst was stirred at constant temperature on a water bath. Previously thermostated H_2O_2 was injected through a silicon stopper, and the evolved O_2 was volumetrically measured.

2.6. SOD indirect assay

The SOD activity of the complexes was assayed by measuring the inhibition of the photoreduction of nitro blue tetrazolium (NBT), by a method slightly modified from that originally described by Beauchamps and Fridovich [38]. The solutions containing riboflavin (3.3×10^{-6} M), methionine (9.5×10^{-3} M), NBT (4.2×10^{-5} M) and the complex of various concentrations were prepared with phosphate buffer (pH 7.8). The mixtures were illuminated by a fluorescent lamp with a constant light intensity at 25 °C. The reduction of NBT was monitored at 560 nm with various illumination periods (t). Rates in the absence and in the presence of different concentrations of complex were determined and plotted vs. complex concentration. Inhibition percentage was calculated according to: $\{(\Delta Abs / t)_{without\ complex} - (\Delta Abs / t)_{with\ complex}\} \times 100 / (\Delta Abs / t)_{without\ complex}$. The IC_{50} value represents the concentration of the SOD mimic that induces a 50% inhibition of the reduction of NBT. On the basis of competition with NBT, at 50% inhibition, the rates of the reactions of $O_2^{\bullet -}$ with NBT and the mimic are equal, k [complex] = k_{NBT} [NBT], where k_{NBT} (pH = 7.8) = 5.94×10^4 M^{-1} s^{-1}[39,40]. Control experiments were performed on mixtures of NBT + complex, riboflavin + complex, and NBT + methionine + complex, in phosphate buffer, to ensure that the complex does not react independently with any of the components of the mixture.

2.7. Crystal data collection and refinement

Single-crystal data were collected on an Oxford Diffraction Gemini E CCD diffractometer equipped with a sealed tube with Mo Kα radiation (λ = 0.71073 Å). Crystal structure data were corrected for absorption with CrysAlisPro, Agilent Technologies, version 1.171.36.28 (**1**·H_2O) and 1.171.34.49 (**3**·2DMSO), applying an empirical absorption correction using spherical harmonics, implemented in SCALE3 ABSPACK scaling algorithm. The structure were solved by direct methods with SIR-92 [41] and refined by full-matrix least-squares on F^2 with SHELXL-2014 [42]. All non-H atoms were refined with anisotropic displacement parameters. The H atoms on carbon atoms were refined isotropically at calculated positions using a riding model. For compound **1**, hydrogen atoms bonded to O atoms, were located in a difference Fourier maps and refined using distance restraints [O—H = 0.85 (1) Å] with $U_{iso}(H) = 1.5U_{eq}(O)$. For compound **3**, the solvent molecule was disordered over two positions with the occupation ratio 0.7:0.3. The atom ellipsoids were restrained to be similar using the SIMU and DELU commands. Crystal data collection and refinement parameters for compounds **1**·H_2O and **3**·2DMSO are summarized in Table 1.

3. Results and discussion

3.1. Solid state studies

Complexes $[Mn(3,5\text{-}F_2salpn)(H_2O)_2][B(C_6H_5)_4]\cdot 2H_2O$ (**1**·$2H_2O$) and $[Mn(3,5\text{-}Cl_2salpn)(OAc)(H_2O)]\cdot H_2O$ (**2**·H_2O) were prepared from 1:1 mixtures of the ligand with $Mn(OAc)_2$ in methanol. While complex **2** precipitates from the reaction mixture, complex **1** required the addition of the bulky BPh_4^- to separate from the solution. Color changes were observed immediately after mixing. When $Mn(ClO_4)_2$ was used instead of acetate, no color change was observed until a base was added to the solution of complex, revealing the role of acetate to deprotonate the phenol group and thus to induce its coordination to the metal center, an event accompanied by a facilitated aerobic oxidation of the Mn^{II}[43–46].

Complexes **1** and **2** share some similar features in the IR spectra, exhibiting a strong band between 1620 and 1612 cm^{-1} characteristic of the $\nu_{C=N}$ stretching mode, which is shifted ≈20 cm^{-1} lower respect to the free Schiff-base ligand, indicating the coordination to the manganese through the nitrogen atoms of the imine group. The peak at 1331 (3,5-F_2salpn)/1356 (3,5-Cl_2salpn) cm^{-1}, assigned to O—H in plane bending vibration of the phenol groups in the free ligands, is absent in the spectra of the complexes, indicating that deprotonated phenol groups are bound to manganese. Besides, the two compounds show strong absorptions centered at 3472/3430 cm^{-1} corresponding to the ν_{OH} stretching of the water molecules. Complex **1** exhibits out-of-plane C—H_{Ar} bending at 738, 708 and 612 cm^{-1}, and strong C—H_{Ar} stretching at 3050 cm^{-1}, characteristic of the non-coordinated BPh_4^- counter-ion. Powdered samples (**1**·$2H_2O$) and crystals of **1**·H_2O display identical IR spectra. Complex **2** shows two additional bands at 1554 and 1392 cm^{-1} assigned to asymmetrical and symmetrical carboxylate CO_2^- vibrational modes of bound acetate, respectively.

Table 1
Crystal data for $[Mn(3,5\text{-}F_2salpn)(H_2O)_2]BPh_4\cdot H_2O$ (**1**·H_2O) and $[(3,5\text{-}Cl_2salpn)_2Mn_2(O)_2]\cdot$2DMSO (**3**·2DMSO).

Empirical formula	$BC_{41}H_{38}F_4Mn\ N_2O_5$	$C_{38}H_{36}Cl_8Mn_2N_4O_8S_2$
M	780.48	1134.31
Temperature	273 K	293 K
Wavelength	0.71073 Å	0.71073 Å
Crystal system, space group	Monoclinic, $P2_1/c$	Triclinic, P-1
Unit cell dimensions	a = 17.0227(10) Å, b = 11.7012(6) Å, c = 19.3517(14) Å α = γ = 90.000(5)°, β = 107.115(7)°	a = 11.094(2) Å, b = 11.3877(16) Å, c = 11.501(2) Å α = 83.731(13)°, β = 70.305(16)°, γ = 61.205(16)°
V	3683.9(4) A^3	1196.3(4) A^3
Z, ρ_{calc}	4, 1.407 Mg/m^3	1, 1.574 Mg/m^3
μ_{Mo}	0.427 mm^{-1}	1.114 mm^{-1}
F(000)	1616	574
θ range for data collection	3.65 to 25.03°	3.60 to 28.86°
Limiting indices	−20 ≤ h ≤ 20, −13 ≤ k ≤ 13, −23 ≤ l ≤ 18	−13 ≤ h ≤ 13, −13 ≤ k ≤ 13, −13 ≤ l ≤ 13
Reflections collected/unique	17,224/6483 [R(int) = 0.0466]	15,520/4376 [R(int) = 0.0797]
Data/restraints/parameters	6483/6/505	4376/114/318
Goodness-of-fit on F^2	1.077	1.049
Final R indices [I > 2σ(I)]	R_1 = 0.0605, wR_2 = 0.1525	R_1 = 0.0721, wR_2 = 0.1834
R indices (all data)	R_1 = 0.0987, wR_2 = 0.1754	R_1 = 0.1053, wR_2 = 0.22
Largest diff. peak and hole	0.62/−0.277 e·A^{-3}	1.13/−0.717 e·A^{-3}

Crystals of **1**·H_2O suitable for X-ray diffraction studies separated from a methanol solution of **1**·$2H_2O$. The molecular structure is shown in Fig. 1. The compound crystallizes in the $P2_1/c$ space group with the asymmetric unit containing a discrete Mn^{III} complex cation, non-coordinated BPh_4^- anion and one solvate water molecule. The fully deprotonated tetradentate Schiff base ligand is tightly bound to the Mn ion via the N_{imine} and $O_{phenolato}$ atoms, with two capping water molecules completing the coordination sphere of the metal centre. The Mn atom is in an axially elongated octahedral environment, with the Mn—O(3), Mn—O(5) bond distances (av. 2.225 Å) distinctly longer than the equatorial Mn—(O1), Mn—O(4), Mn—N(1) and Mn—N(2) ones (av. 1.968 Å). These values are consistent with Jahn–Teller elongation of a d^4 Mn^{III} ion in an octahedral ligand field, and are comparable to those reported for other Mn^{III} Schiff-base complexes [30,44,47,48]. The values of the *trans*-angles in the coordination environment of the Mn ion are between 173.83 and 175.10°, indicating a weak distortion from pure octahedral geometry.

Complex cations are associated in pairs through H-bonds and π-aryl interactions as shown by O—H···O short contacts between capping water and the two $O_{phenolato}$ atoms of the neighboring Schiff-base, with distances O(5)H···O(1) = 2.85 Å and O(5)H···O(4) = 2.92 Å (Fig. 2). This results in a short Mn···Mn distance of 4.93 Å typical of μ-aqua dimers [13,43,49,50]. There is an additional intermolecular H-bond between the other coordinated H_2O molecule and the solvate water with distance O(3)H···O(0aa) 2.72 Å. H-π interaction between the bound water molecule and the phenyl ring of BPh_4^-, with a centroid-to-O(3) distance of 3.40 Å, provides a plausible reason for the short O(3)H···O(0aa) length. Aromatic rings of the two neighboring complex cations interact through π-π stacking, with a centroid-to-centroid distance of 3.70 Å between overlapping rings. The pairs of complex cations are isolated from each other by the BPh_4^- anions. The crystal packing probably results from Van der Waals interactions.

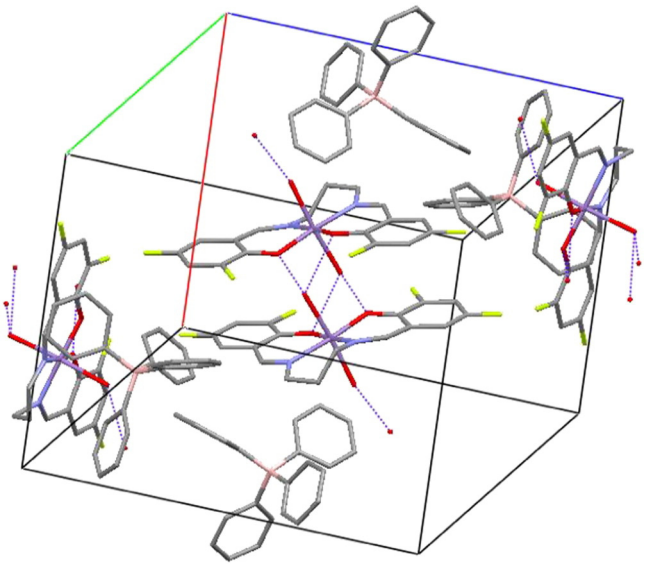

Fig. 2. Crystal packing diagram for **1**·H_2O, emphasizing the intermolecular hydrogen-bonding interactions.

3.2. Solution studies

The specific conductivity of 1.0 mM solutions of the complexes was measured in methanol. The molar conductivity for **1** is 55 Ω^{-1} cm^2 mol^{-1}. This value is the expected for a complex that contains the low mobility BPh_4^- anion and behaves as 1:1 electrolyte in solution [51]. In line with this, the ESI-mass spectrum of a freshly prepared solution of **1** in DMF shows only one peak (negative) at m/z = 319 corresponding to BPh_4^- anion, and two main peaks (positive) at m/z = 407.4 (100%) and 480.3 (99%) belonging to MnL^+ and $MnL(DMF)^+$ (Fig. 3(a)), respectively. No traces of free ligand or dimeric species were found. The diamagnetic ^1H NMR spectrum of **1** in D_4-methanol shows peaks belonging to the aromatic protons of BPh_4^- without traces of the Schiff-base ligand (Fig. S1), indicating the complex is stable towards metal dissociation even in a protic solvent.

For **2**, the molar conductivity of the equilibrated methanol solution is 46 Ω^{-1} cm^2 mol^{-1}, thus revealing partial dissociation of coordinated acetate with time, in the protic solvent.

The paramagnetic ^1H NMR spectra of **1** and **2** in D_4-methanol (Fig. 4) reveal a simple pattern for the two complexes outside the diamagnetic region (ca. 0–10 ppm). In both cases, one broad resonance is observed at 19 ppm corresponding to the central —CH_2— of the aliphatic chain. A second resonance appears up-field at −14.3 (**1**) and −16.2 ppm (**2**), which can be assigned to the H4 aromatic ring proton on the basis of comparison with reported spectra for other phenolato-based Mn^{III}

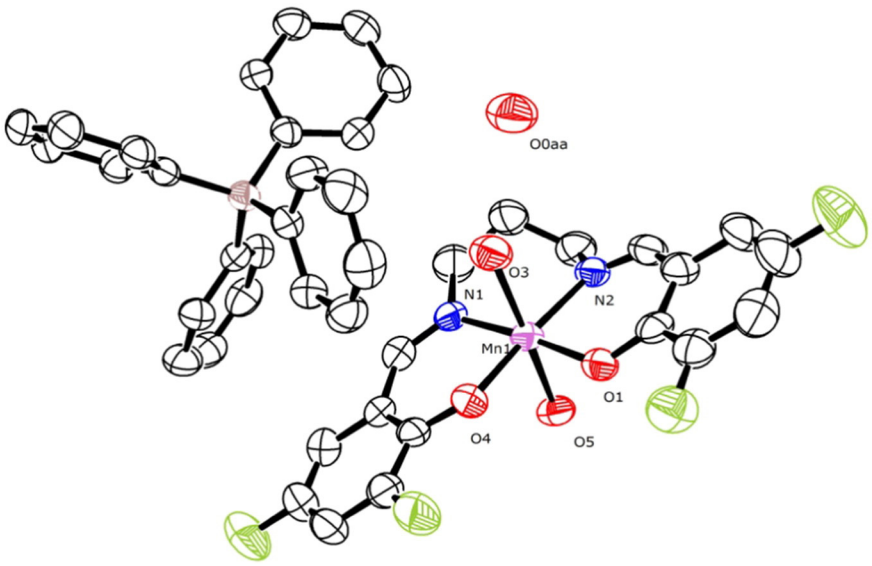

Fig. 1. Plot of the asymmetric unit of **1**·H_2O at the 50% probability level. Hydrogen atoms have been omitted for clarity. Selected bond lengths (Å) and angles (°): Mn(1)—O(1) 1.893(3), Mn(1)—O(4) 1.901(3), Mn(1)—O(5) 2.239(3), Mn(1)—N(1) 2.057(4), Mn(1)—N(2) 2.019(4), Mn(1)—O(3) 2.210(3). O(1)—Mn(1)—N(1) 175.00(14), O(4)—Mn(1)—N(2) 175.10(15), O(3)—Mn(1)—O(5) 173.83(14).

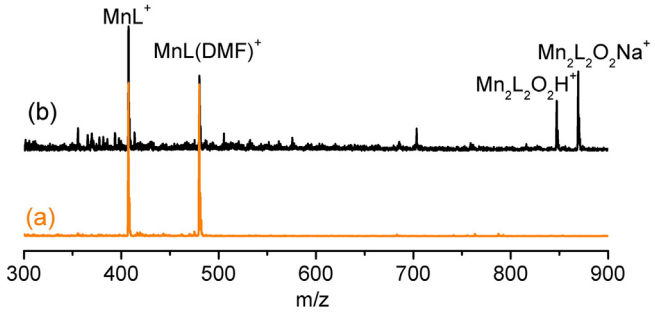

Fig. 3. ESI-mass spectra of (a) freshly prepared solution of **1** in DMF, (b) solution of **1** in DMF, 48 h after prepared.

complexes [52,53]. Because of their closeness to the Mn centre, protons adjacent to the donor groups of the Schiff base ligand (aromatic H6, N═CH— and —CH_2—N═C) are not observed, and this is consistent with previous finding for related Mn^{III} complexes [54]. Paramagnetic ^{1}H NMR is a useful probe of the ligand conformation of Mn-Schiff-base complexes in solution. The observation of only one resonance for the aromatic ring protons in the ^{1}H NMR spectra of **1**–**2** indicates that these complexes possess trans-diaxial symmetry with the tetradentate Schiff base ligand symmetrically arranged in the equatorial plane [52,55–57]. A more complex pattern is expected when the ligand adopts a *cis*-α or *cis*-β folded conformation because the different extent of charge transfer for protons of the phenolato *trans* to different groups results in the magnetic nonequivalence of protons of the two phenolato rings [52, 58]. The chemical shift of H4 correlates with the Hammett parameter of the aromatic *p*-substituent (σ_p): δ_{H4} is larger for the complex with the more electron-withdrawing group, as shown in the inset of Fig. 4 where the complex with the NO_2 derivative is included. This trend in the chemical shifts as a function of the aromatic substituent (NO_2 > Cl > F) indicates that these ligands are predominantly π-donor and correlates with the strength of the phenolato-Mn bond: thus, the stronger the electron-withdrawal from the $O_{phenolato}$, the stronger the Mn-ligand bond and the larger the contact shift on H4.

The paramagnetic ^{19}F NMR spectrum of complex **1** in D_4-methanol affords two peaks confirming the symmetrical disposition of the ligand around the Mn ion (Fig. S2). The peaks at −127 (F5) and −135 (F3) ppm (vs Cl_3CF) in the free ligand, were assigned to F5 and F3, respectively, based on the coupling pattern (Figs. S3 and S4). In the complex, these peaks broaden and shift to −75 (F5) and −60 (F3) ppm.

The paramagnetic ^{1}H NMR spectra of freshly prepared solution of **2** in D_7-DMF (Fig. S5) also exhibit a simple pattern outside the diamagnetic region with an up-field resonance at −8 ppm corresponding to H4, which is not modified after addition of base. This indicates that **2** retains the *trans* geometry in DMF and basic DMF [53].

The mass spectrum of a freshly prepared DMF solution of **1** shows peaks at *m/z* 407.4 (MnL^+) and 480.3 ($MnL(DMF)^+$). With time, new peaks appear at *m/z* 847.5 and 869.6, corresponding to the Mn^{IV}_2 dimeric species $Mn_2L_2O_2H^+$ and $Mn_2L_2O_2Na^+$, respectively. After 48 h, the relative intensities of peaks belonging to monomeric and dimeric species are: 100% MnL^+, 60% $MnL(DMF)^+$, 40% $Mn_2L_2O_2H^+$ and 64% $Mn_2L_2O_2Na^+$ (Fig. 3(b)). The same behavior was observed in DMSO. These results reveal this complex is prone to form the high valence dimer in air, although the rate is slow. This was confirmed through spectrophotometric monitoring of a solution of **1** in DMF and basic DMF. In this solvent the complex shows a band at 375 nm corresponding to a L → M charge transfer transition from pπ orbitals of the phenolato oxygen to the partially filled dπ orbitals of the Mn^{III} ion [44,59,60], and a broad band centered at 550 nm (ε 265 M^{-1} cm^{-1}) that can be assigned to a d–d transition of Mn^{III} in a pseudotetragonal environment [13,44]. Addition of base (up to 10 equiv.) shifts the ligand to metal charge transfer (LMCT) band to 370 nm. When left in air, the spectrum does not alter immediately, but after several hours a new broad band grows up at 460–550 nm, which can be attributed to the formation of the high-valence oxo-bridged diMn dimer [61–63]. In neat DMF, the intensity of this band raises slower than in basic DMF. The spectrum of a solution of **1** + 10 equiv. of base registered after 1 day is shown in Fig. 5. When 20 or more equiv. of base are added, the band at 460–550 nm clears up and the intensity of the LMCT band at 370 nm increases (Fig. 5(b)), probably because of the formation of the $[Mn(F_2\text{-salpn})(OH)_2]^-$ complex. Deoxygenated DMF solutions of **1**, do not evolve with time.

The formation of the Mn^{IV} dimer was also verified for **2** in DMSO. Several days after preparing the solution and left in air, crystals of $[Mn_2(3,5\text{-}Cl_2salpn)_2(O)_2]\cdot 2DMSO$ (**3**·2DMSO) separated from the solution, the structure of which was confirmed by X-ray diffraction. The molecular structure of **3**, shown in Fig. 6(a), consists of a binuclear Mn complex bridged by two oxo groups and two Schiff-base ligands acting as *N,O*-donors to each manganese centre, resulting in a Mn···Mn separation of 2.7239(15) Å. Each Mn atom is in a hexacoordinate environment [MnN_2O_4], with two $O_{phenolato}$ from the two 3,5-Cl_2salpn ligands and two bridging oxo ligands occupying the equatorial plane of a distorted octahedron. The axial sites of the Mn atoms are occupied by two N_{imino}, each one from a different Schiff-base ligand. Bond distances Mn(1)—O(2) 1.809(3) Å, Mn(1)—O(2^i) 1.812(3) Å, Mn—$O_{phenolato}$(av)

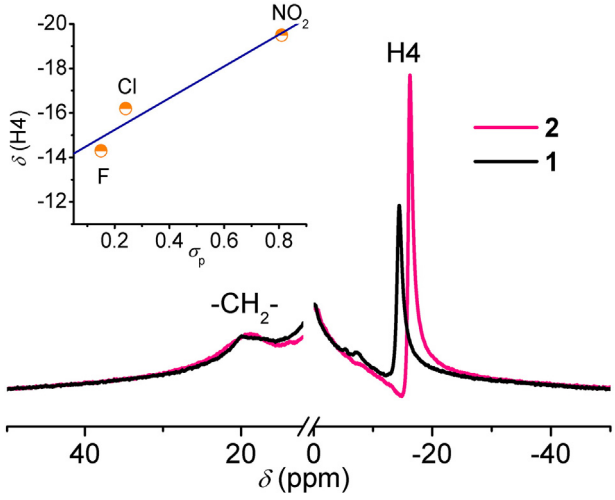

Fig. 4. ^{1}H NMR spectra of 13 mM **1** and 16 mM **2** in D_4-methanol at 26 °C. Inset: correlation of δ_{H4} with σ_p of the substituent.

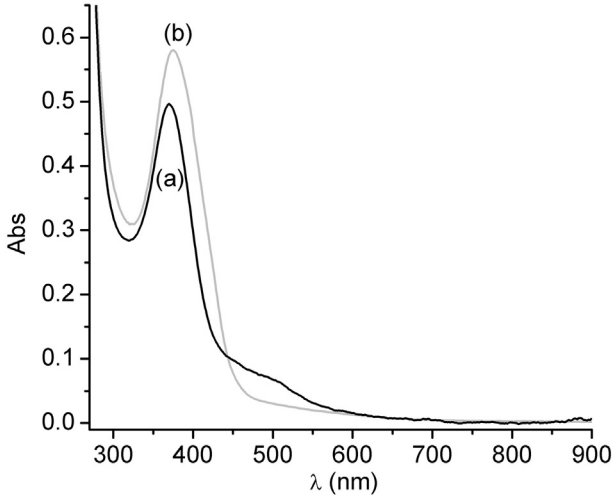

Fig. 5. (a) 50 μM **1** + 10 equiv. Bu_4NOH in DMF, *t* = 24 h; (b) 50 μM **1** + 30 equiv. Bu_4NOH in DMF; *t* = 24 h.

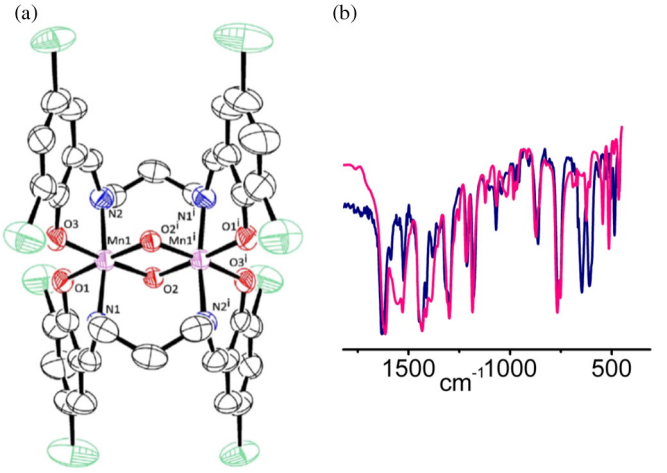

Fig. 6. (a) Molecular structure of the Mn^{IV}_2 dimer **3**. Selected bond lengths (Å) and angles (°): Mn(1)—O(2) 1.809(3), Mn(1)—O(1) 1.932(3), Mn(1)—O(3) 1.921(3), Mn(1)—O(2^i) 1.812(3), Mn(1)—N(1) 2.024(4), Mn(1)—N(2) 2.009(4), Mn(1)···Mn(2) 2.7239(15). Mn(1)—O(2)—Mn(1^i) 97.56(13), O(2)—Mn(1)—O(3) 174.49(14), O(1)—Mn(1)—O(2^i) 173.09(13), N(1)—Mn(1)—N(2) 172.39(16). (b) IR spectra of **3** (▬) and **2** (▬). *Band from the ligand.

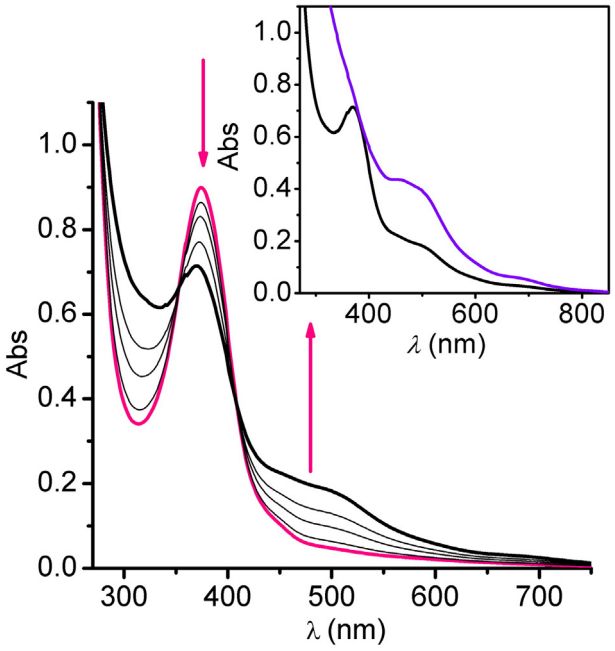

Fig. 7. Electronic spectra of 50 mM **2** in DMF at different time-intervals: $t = 0$ (▬), 6, 12, 18 and 24 h. Inset: Spectra of (▬) **2** in DMF after 24 h and (**violet line**) **3** in MeCN.

1.927 Å and Mn—N_{imine}(av) 2.017 Å are consistent with a di-μ-oxo-bridged Mn^{IV} complex [36,44,50,64–65] and are similar to the DMF adduct $[Mn_2(Cl_2\text{-salpn})_2(\mu\text{-O})_2]\cdot 4.5DMF$ previously characterized by X-ray diffraction [66].

Solutions of **2** in DMF, MeCN and DMSO were left in air and the IR spectra of the separated solids compared. It must be noted that the relative rate of precipitation is well different in the three solvents -MeCN ≫ DMSO > DMF-, so in DMF and DMSO solids were collected after several days. The IR spectra of the three solids –which are essentially superimposable to the spectrum of a crystalline sample of **3**·2DMSO- exhibit a sharp absorption band at 647 cm^{-1} attributable to the highly symmetrical $\{Mn_2O_2\}$ core with the $O_{phenolato}$ occupying the positions *trans* to the two Mn—O_{oxo} bonds [36,67]. Therefore, the same dimer with the bridging Schiff-base ligand (**3**) forms in the three solvents (although at different rates), the IR spectrum of which is well different from that of the starting complex **2**, particularly in the regions of ν_{OAc} and low frequencies (Fig. 6(b)).

The electronic spectrum of complex **2** in DMF shows an intense phenolato to Mn charge transfer band at 374 nm, a shoulder at 440 nm and a low intensity broad absorption centered at 505 nm. The LMCT band decreases with time while three broad bands at 450, 500 and 680 nm grow up (Fig. 7). A similar behavior is observed when up to 10 equiv. of Bu_4NOH are added to the DMF solution of **2**. Higher excess of base depletes the bands at longer wavelengths and enhances absorbance at 367 nm, as observed for **1**, a fact also verified in DMSO. The bands at 450, 500 and 680 nm are the signature of the formation of **3** as shown in the inset of Fig. 7, where the DMF spectrum of a solution of **2** aged 24 h is compared to the spectrum of **3** in MeCN.

These results confirm that the formation of **3** in DMF is a slow process that requires several days for completion.

3.3. Electrochemical studies

The electrochemical properties of complexes **1**–**2** were investigated by cyclic voltammetry in DMSO, DMF and MeOH (Fig. 8, S6–S8). The two complexes exhibits one quasi-reversible wave with $E_{1/2}$ in the range −27 to 101 mV vs. SCE (depending on the solvent, Table 2), with ΔE_p = 120–160 mV and Ia/Ic ~0.9, corresponding to the Mn^{III}/Mn^{II} redox couple of the complexes. These $E_{1/2}$ values can be correlated with the donor numbers (DN) of the three solvents; DN: 29.8 (DMSO) > 26.6 (DMF) > 19 (MeOH). Thus, the higher oxidation state

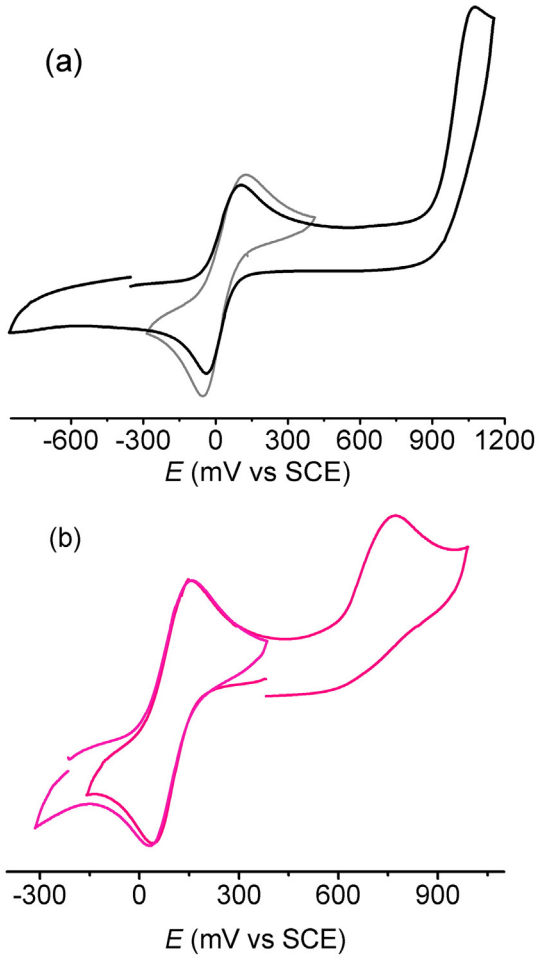

Fig. 8. Cyclic voltammograms of (a) **1**, and (b) **2**, in DMF. [complex] = 1 mM. Supporting electrolyte = Bu_4NPF_6. Scan rate = 100 mV s^{-1}, working electrode = Pt.

Table 2
Reduction potentials for the Mn^{III}/Mn^{II} couple of Mn-salpn and Mn-salen type complexes.

	Compound	$E_{1/2}$ (mV vs SCE) Mn^{III}/Mn^{II}	E_p (mV vs SCE) Mn^{III}/Mn^{IV}	Solvent	Reference
1	**1**	−27	–	DMSO	This
		37		DMF	work
		86		MeOH	
2	**2**	24	772	DMSO	This
		94		DMF	work
		101		MeOH	
3	[Mn(3,5-Cl_2salpn)]ClO_4	71	–	DMF	[36]
4	$[Mn(salpn)]^+$	−154	–	DMSO	[44]
		−106	–	MeCN	[53]
5	[Mn(salpn)(OAc)]	−270	980	Cl_2CH_2	[68]
6	[Mn(salpn)Cl]	−125	905	MeCN	[69]
7	[Mn(3,5-Cl_2salen)]ClO_4	31	–	DMF	[50]
8	[Mn(salen)]ClO_4	−225	–	DMF	[50]
9	[Mn(salen)Cl]	−245	895	MeCN	[69]
10	[Mn(3-OMe-salen)$(H_2O)_2$]NO_3	−237	–	DMF	[70]
11	[Mn(3-OMe-salen)(OAc)]	−255	–	DMSO	[11]

of Mn is more stabilized in the solvents with higher DN values. As expected, the Mn^{III}/Mn^{II} redox potential increases with the inductive effect of the electron-withdrawing substituent on the phenolato ring; thus, the Cl-substituted complex (**2**) is easier to reduce than the F-substituted one (**1**). The $E_{1/2}$ for the Mn^{III}/Mn^{II} couple of **2** occurs at a potential 23 and 63 mV higher than for [Mn(3,5-Cl_2-salpn)]ClO_4 and [Mn(3,5-Cl_2-salen)]ClO_4, respectively. Salen complexes are reduced at more negative potential than the salpn analogues which possess a more flexible propylene spacer between the imino groups that destabilizes the Mn^{III} state with respect to reduction (Table 2, entries 3, 7).

In the anodic scan of **1**, the BPh_4^- oxidation appears as an irreversible peak at $E_p \approx 1062$ in DMF and 1040 mV in DMSO.

For complex **2** in DMF, an additional nonreversible oxidation peak is observed at $E_p = 772$ mV in the anodic scan (Fig. 8(b)), attributable to the Mn^{III}/Mn^{IV} couple. This stabilization of the Mn^{IV} oxidation level is likely the result of the presence of the basic acetate coordinated to the metal. The stabilizing effect of the axial anionic ligand had already been observed for other Mn-salpn(X) and Mn-salen(X) complexes (Table 2, entries 5, 6, 9; X = axial substituent), which are oxidized below 1 V. Addition of acid to the DMF solution of **2** causes disappearance of the wave at 772 mV (Fig. S9(b)), shift of the Mn^{III}/Mn^{II} couple to a slightly lower potential ($E_{1/2} = 71$ mV) and emergence of the reduction peak of dissociated acetatic acid in the cathodic scan. Subsequent addition of Bu_4NOH restores the Mn^{III}/Mn^{IV} wave (Fig. S9(c)). The oxidation of unbound acetate at 772 mV was discarded based on the lack of such an oxidation peak in DMF solution of NaOAc and the high oxidation potential value reported for acetate [71].

Voltammograms registered after addition of substoichiometric amounts of Bu_4NOH to a freshly prepared DMF solution of **1**, show the wave corresponding to the Mn^{III}/Mn^{II} couple at 37 mV and an oxidation peak at 707 mV (Fig. S10), which might result from the conversion of the starting complex into the hydroxo-Mn^{III} complex [72]. The hydroxo group stabilizes the high oxidation state of the metal favoring the oxidation to $[Mn^{IV}(OH)(3,5\text{-}F_2salpn)]^+$ at a potential much lower than for the cationic complex [44] but does not affect the Mn^{III}/Mn^{II} couple significantly (entries 4/6, 8/9, 10/11 in Table 2). Voltammograms of freshly prepared solutions of complexes **1** and **2** in DMF and basic DMF, exclude the formation of oxo-bridged diMn dimers at short times, the signature of which is significantly different [44,73–75].

3.4. SOD activity

The complexes' stability was checked by UV–vis spectroscopy in the aqueous phosphate buffer employed for the SOD test. Electronic spectra of complex **1** registered at different time–lengths (up to 2 h) after preparation of the solution were identical (Fig. S11(a)), revealing the compound is stable in the buffer. The electronic spectra of **2** in phosphate buffer change with time, probably as a consequence of acetate/hydroxide substitution in the aqueous basic medium. However, spectral changes are slow. So, if the SOD activity is measured with the freshly prepared solution, most acetate is still bound to Mn as revealed by the minor changes observed in the electronic spectra registered during the first 45 min after preparing the solution (Fig. S11(b)). After 24 h, the spectral pattern of **2** is similar to that of **1** and can be attributed to [Mn(3,5-Cl_2salpn)OH] formed through acetate replacement by hydroxide.

The SOD activity of complexes **1**–**2** was determined in aqueous buffer of pH 7.8 using the NBT assay, which is based on kinetic competition between NBT and the complex for reacting with $O_2^{\bullet -}$. In this assay SOD activity is inversely related to the amount of formazan, the purple product formed by the reaction of NBT with $O_2^{\bullet -}$, observed at 560 nm. The two complexes inhibit the reduction of NBT with increasing inhibition as the concentration of complexes increases, as shown in Fig. 9. The IC_{50} values, graphically evaluated, are 2.72 and 3.22 μM and the rate constants, $k = k_{NBT}$ [NBT] / IC_{50}, are shown in Table 3. These k values are independent of the detector concentration and appropriate for comparison with other catalysts.

Based on k, the activity of **1**–**2** is in the range of other Mn complexes of tetradentate Schiff-base ligands (Table 3), meaning that ring substitutions and spacer length modifications have little effect on the SOD activity of this kind of Mn complexes. SOD activity seems to be more related to the solubility of the complex. In this way, water soluble Mn complexes of sulfonato-derived ligands (Table 3) react faster than **1** and **2**, even when the last two complexes possess metal-centered redox couples closest to the midpoint between the oxidation and reduction of $O_2^{\bullet -}$ (120 mV vs. SCE).

3.5. CAT activity

The ability of complexes **1**–**2** to catalyze H_2O_2 disproportion was tested in basic DMF. In these studies, solutions of catalyst were prepared in degasified solvent and used immediately to ensure only monomeric species are present when H_2O_2 is added. Without addition of base, the reaction rates are extremely slow. Addition of H_2O_2 to a solution of the catalyst + Bu_4NOH in DMF causes evolution of dioxygen coupled to color change from brown to orange. In the presence of 10 equiv. of Bu_4NOH, complexes **1**–**2** were able to disproportionate up to 58 and 115 equiv. of H_2O_2, respectively. These TON values, although low, are higher than reported for other Mn-Schiff-base complexes in protic solvent (Table 4).

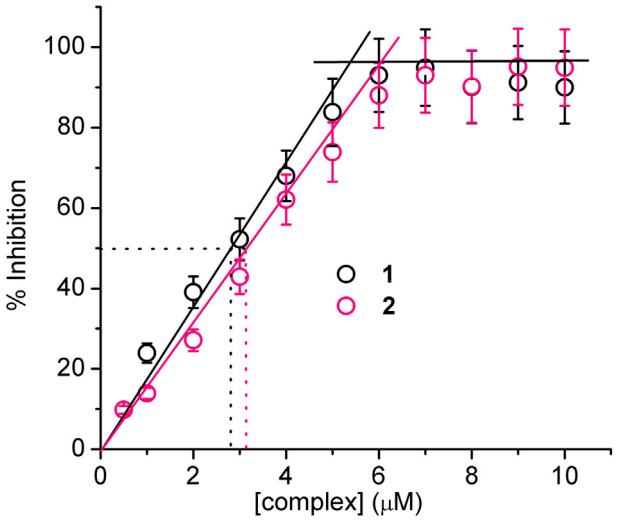

Fig. 9. SOD activity of complexes **1** and **2** in the riboflavin-methionine-NBT assay.

Table 3
SOD activity of **1**–**2** and other Mn-Schiff-base complexes.

Complex	SOD activity		SOD test	Ref.
	IC_{50} (μM)	10^{-6} k_{McCF} (M^{-1} s^{-1})		
1	2.72	0.92	pH 7.8[a]	This work
2	3.22	0.77	pH 7.8[a]	This work
[Mn(X-salen)(AcO/Cl)]	0.7–1.3	0.6	pH 7.8[b]	[7,9,10]
[Mn(3-OMe-salenR)(OAc)]	0.044–0.146	–	pH 7.4[c]	[11]
Na[Mn(SO_3-salpn)]	0.77	3.6	pH 7.8[a]	[12]
Na[Mn(SO_3-salen)]	2.34	1.17	pH 7.8[a]	[12]
K_2[Mn(SO_3-Cysalen)(OAc)]	2.68	5.49	pH 7.8[b]	[76]
[Mn(salbutO)N_3]	1.43	1.91	pH 7.8[a]	[14]

X = H, F, OMe, OEt. R = cyclopentane-fused with ureido or acid–base catalyst auxiliary. SO_3-CySalen = *N*,*N*′-bis(5-sulfonatosalicylidene)-(*R*,*R*)-1,2-diaminocyclohexane. SalbutOH = 1,4-bis(salicylidenamino)butan-2-ol.
[a] Riboflavin–methionine–NBT assay.
[b] Xanthine–xanthine oxidase–NBT assay.
[c] Xanthine-xanthine oxidase-cytochrome *c* assay.

The initial rate of H_2O_2 disproportionation (r_i) by **1** + Bu_4NOH in DMF was measured as a function of the complex and substrate concentrations at 25 °C. In this medium, at constant $[H_2O_2]_0$, r_i shows quadratic dependence on $[\mathbf{1}]_0$ (Fig. 10), with second-order rate constant k_1" = 24.2(4) mM^{-1} s^{-1} ($[H_2O_2]_0$ = 10 mM). At constant $[\mathbf{1}]_0$, the initial rate of H_2O_2 dismutation exhibits saturation kinetics with $[H_2O_2]_0$ (Fig. 10), and the experimental data could be modeled by the Michaelis–Menten equation from which the maximum rate V_{max} = 0.034(2) mM s^{-1} and the Michaelis constant K_M = 1.5(1) mM, were determined.

Room-temperature UV–vis absorption spectra were taken during the progress of the reaction of complex **1** with 150 equiv. of H_2O_2 in basic DMF (Fig. 11). Immediately after H_2O_2 addition, the 370 nm band of complex **1** decreases and a shoulder appears at 405 nm (brown line in Fig. 11). The intensity of this shoulder rapidly diminishes concurrently with the apparition of a broad band in the range 450–550 nm (orange line in Fig. 11). As the reaction progresses the solution becomes turbid, probably resulting from the formation of a poorly soluble inactive or degraded form of the complex. The absorption in the 450–550 nm region holds during the reaction, and based on the above discussion, might correspond to a di-μ-oxo-bridged diMn dimer in accordance with the peak at *m*/*z* 847.5 in the ESI-mass spectrum taken on a reaction mixture (Fig. 11, inset). Notably, the reaction mixtures are EPR silent. No mononuclear Mn^{IV}, which would be expected to have a feature near *g* = 4, nor $Mn^{III}Mn^{IV}$ mixed-valence species characterized by 16-line spectrum centered at *g* = 2, are observed, during or at the end of the reaction.

For complex **2**, the initial rate of H_2O_2 disproportionation in basic DMF shows second-order dependence on $[\mathbf{2}]_0$ (Fig. 12(A)), with k_2" = 1.84(5) mM^{-1} s^{-1} at saturating substrate concentrations. The electronic spectra registered on a reaction mixture of 50 equiv. of

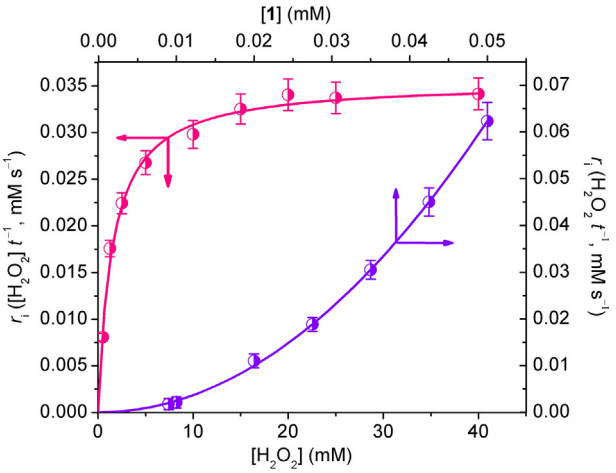

Fig. 10. Effect of the $[H_2O_2]$ (pink line; [catalyst] = 35 μM) and [catalyst] (violet line; $[H_2O_2]$ = 10 mM) on the initial rate of H_2O_2 disproportionation catalyzed by **1**, at 298 K, in DMF solution of 0.35 mM Bu_4NOH. (For interpretation of the references to color in this figure legend, the reader is referred to the web version of this article.)

H_2O_2 over catalyst (Fig. 12(B)) show the decrease of the band at 367 nm, corresponding to the starting complex, the appearance of a new band at 423 nm and a shoulder at ~445 nm. After reacting with 100 equiv. of H_2O_2, the band at 367 nm disappears completely giving rise to the band at 423 nm. The reaction mixture remains clear until the end of O_2 evolution, without traces of solid. Upon addition of NH_2OH, the band at 423 nm converts into two bands at 367 and 320 nm (inset in Fig. 12(B)). Further addition of NH_2OH causes the vanishing of absorptions at 367 and 423 nm and growth of the band at 320 nm. At the end of the H_2O_2 disproportionation reaction, the catalyst is EPR silent, but the species generated by complete reduction with NH_2OH shows the six-line signal at *g* = 2 typical of non-coupled Mn^{II}.

Second-order dependence of the initial reaction rate on [catalyst] implies the involvement of two molecules of the complex at (or before) the slow step of the catalytic cycle. Based on kinetics and spectroscopic results, a plausible mechanism for H_2O_2 disproportionation by complexes **1** and **2** is proposed in Scheme 2. The reaction starts upon binding of peroxide to the hydroxo (or acetato) Mn^{III} complex, $LMn^{III}X$ (X = OH or OAc), through substitution of the hydroxo/acetato group followed by reaction with a second $LMn^{III}X$ (X = OH or OAc) molecule to yield the oxidized active form of the complex that initiates the catalytic cycle: a high-valent $[LMn^{IV}(O)]_2$ species. This is consistent with the observation of an initial time-lag at the onset of the O_2 evolution. The oxidized catalyst reacts with one H_2O_2 molecule in the oxidative half-reaction to yield the reduced active form of catalyst $[LMn^{III}OH]_2$ coupled to O_2 formation, without change in the total formal charge of the catalyst. The so-formed

Table 4
CAT activity of **1**–**2** and other Mn-Schiff-base complexes.

Compound	r_i (mmol H_2O_2 mmol cat^{-1} min^{-1})	TON[b]	Solvent	Ref.
1	14.5	58	DMF + 10 equiv. TBAOH	This work
2	1.1	115	DMF + 10 equiv. TBAOH	This work
[Mn(X-salen)OAc]	11–24[a]	2.5-8.4	H_2O, pH 8.1	[9,10,77]
[Mn(3-OMe-salenR)(OAc)]	8–29[a]	4-17	H_2O, pH 7.4	[11]
$[Mn(Y\text{-salpn})]^+$	–	17–25	CH_3OH	[13]
$[Mn(5\text{-}SO_3\text{-salpn})]^-$	25.2[a]	250	H_2O, pH 8.1	[12]
$[Mn(Z\text{-salpnOH})]^{\pm}$	3.6/178[a]	0.5/250	H_2O, pH 8.1	[9,12]
$[Mn(salpn)(O)]_2$	575[a]	>1000	Cl_2CH_2/CH_3CN	[30]
[Mn(salbutO)N_3]	3.4[a]	1200	DMF	[14]

X = H, OMe, F, OEt. R = cyclopentane-fused with ureido or acid–base catalyst auxiliary. Y = OEt, Cl, Br. Z = 3-OMe, 5-SO_3. SalpnOH = 1,3-bis(salicylidenamino)propan-2-ol. SalbutOH = 1,4-bis(salicylidenamino)butan-2-ol.
[a] r_i values were calculated from reported kinetic data. [catalyst] = 10 μM; $[H_2O_2]$ = 10 mM.
[b] Total mmol H_2O_2/mmol catalyst.

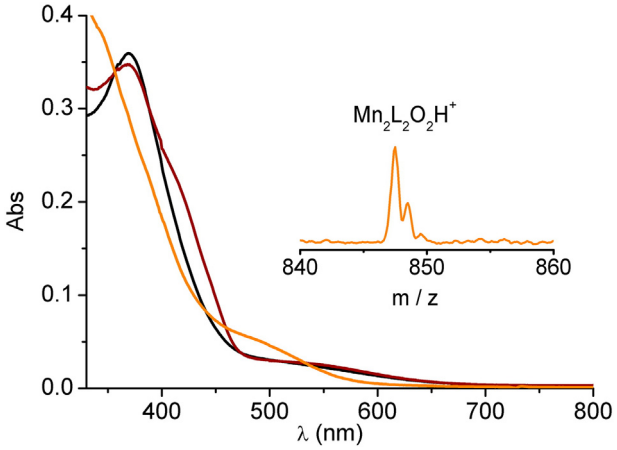

Fig. 11. Electronic spectra of **1** before (▬), immediately after (▬) and 10 min (▬) after addition of 150 eq. H_2O_2 to a solution of 3.5×10^{-2} mM **1** + 10 eq TBAOH in DMF. Inset: peak at *m/z* 847.548 in the ESI-MS spectrum of a reaction mixture. (For interpretation of the references to color in this figure legend, the reader is referred to the web version of this article.)

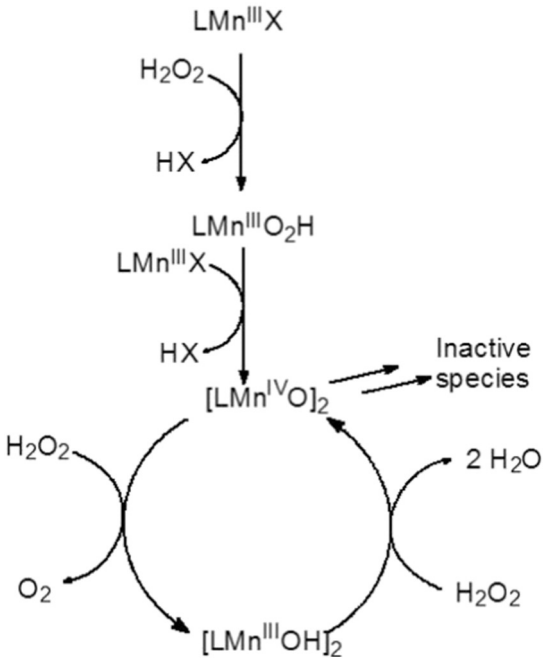

Scheme 2. Proposed mechanism for the reaction of **1** and **2** with H_2O_2. X = OH or OAc.

Mn^{III}_2 complex reacts with another H_2O_2 molecule in the reductive half-reaction to yield water and restore the oxidized active form of the catalyst, thus closing the cycle. The catalytic cycle is proposed to run between Mn^{III}_2 and Mn^{IV}_2 oxidation states which correspond to Mn in configurations that are EPR-silent in perpendicular mode and is consistent with the ability of **1** and **2** to access higher oxidation state in basic medium. The formation of dimeric forms of the catalyst is in agreement with the second order kinetics, the observation of a peak corresponding to the diMn species in the mass spectra and the lack of a peak belonging to the monomer. The low turnover numbers suggest the conversion of the complex into inactive species through a mechanism competitive with catalysis. In the case of complex **1**, these species precipitate from the reaction mixture, while for **2** remain in solution and could correspond to a Mn^{III}_2 inactive form of the complex which can be fully reduced to Mn^{II} with NH_2OH.

The effect of the electron-withdrawing phenyl-ring substituent of **1** and **2** is reflected in their relative redox potentials and reaction rates. Thus, complex **1** which is easier to oxidize in basic medium (E_p = 702 mV) reacts faster than **2** (E_p = 772 mV). In addition, the steric hindrance of the bulkier substituent on C3 of the aromatic ring in **2** can also contribute to reduce the reaction rate. Therefore, both electronic (Hammett constant $\sigma_{p(Cl)} = 0.23$ vs $\sigma_{p(F)} = 0.06$) and steric factors lead **1** to react 14-times faster than **2**. Even if more reactive, complex **1** yields one half of the O_2 evolved by **2**, due to the rapid formation of insoluble inactive species. The initial rate of H_2O_2 disproportionation catalyzed by **1** is in the range of other Mn-Schiff-base complexes in basic media, with the exception of SO_3-subsituted complexes that display higher activity and turnover numbers (Table 4). Complex **2** exhibits the lowest activity among all studied Mn-Schiff-base complexes, a fact mainly attributed to the contribution of the steric effect of the 3-Cl-substituent (*ortho* to the phenolato group) together with the electronic effect of the 5-Cl-substituent. The initial rates measured for mononuclear Mn-Schiff-base complexes are in all cases much slower than reported for the [Mn(μ-O)salpn]$_2$ dimer, which exhibits high catalytic activity without addition of base [30]. The low proportion of the dimer formed in situ upon reaction of the monomer with H_2O_2 may account for the low turnover frequencies of the mononuclear Mn complexes. Besides, unlike CAT studies of mononuclear Mn-Schiff-base complexes, the activity of [Mn(μ-O)salpn]$_2$ was evaluated in anhydrous medium, where hydrolytic inactivation processes are not competitive with catalysis.

4. Conclusions

The reaction of 3,5-F_2salpn and 3,5-Cl_2salpn with $Mn(OAc)_2$ in methanol affords mononuclear $[Mn(3,5\text{-}F_2salpn)]^+$ (**1**) and [Mn(3,5-

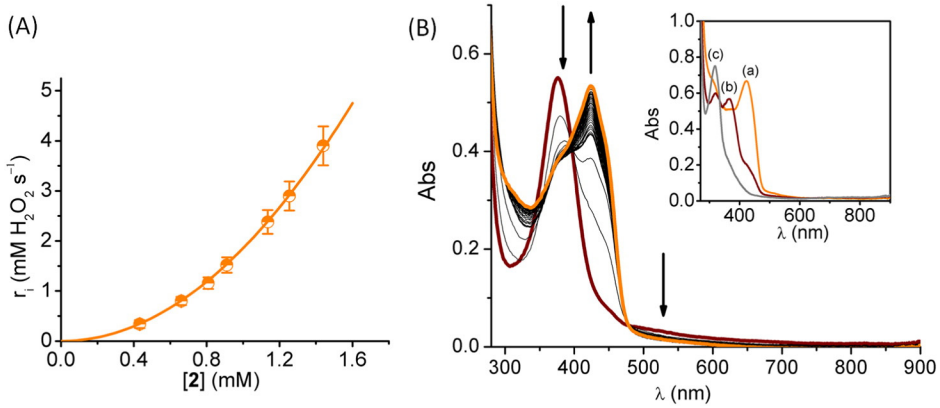

Fig. 12. (A) Effect of the [catalyst] on the initial rate of H_2O_2 disproportionation catalyzed by **2**, at 298 K, in DMF. [H_2O_2] = 0.19 M; Bu_4NOH = 12 mM. (B) Sequential electronic spectra of 3.7×10^{-2} mM **2** + 10 equiv. TBAOH + 50 equiv. of H_2O_2 in DMF. Inset: electronic spectra taken at the end of the reaction of 6.1×10^{-2} mM **2** + 10 equiv. TBAOH + 100 equiv. H_2O_2 (a), after addition of (b) 1.4 μmol of NH_2OH and (c) 2.7 μmol of NH_2OH.

Cl_2salpn)(OAc)] (**2**). When left in air in non protic solvents, both complexes form μ-oxo-Mn^{IV}_2 dimers slowly. Addition of base stabilizes the Mn^{IV} oxidation level upon coordination to the metal and favors the dimerization process. The dimer formation is negligible at short times under anaerobic conditions so that the monomers are the starting species in the CAT/SOD-activity studies. The phenyl-ring substituents of **1** and **2** play an important role on the redox potentials and CAT reaction, but have little effect on SOD activity. Complex **1** with the small and less electron-withdrawing F-substituent is oxidized easier and disproportionate H_2O_2 faster than the 3,5-Cl_2-substituted complex **2**. Second-order kinetics on catalyst, the observation of a lag period at the onset of O_2 evolution, MS and spectroscopic results converge at a catalytic cycle for H_2O_2 disproportionation that runs between Mn^{III}_2 and Mn^{IV}_2 oxidation states. Therefore, complexes **1** and **2** react through a high-valent dimer such as suggested for $[Mn(salpn)]^+$[30] and distinguish from $[Mn(salen)]^+$, with a more rigid and smaller chelate ring, which decomposes H_2O_2 involving mononuclear Mn^{III}/Mn^{V}=O species in the catalytic cycle [9,21–26].

Abbreviations

CAT	catalase
CySalen	*N,N′*-bis(salicylidene)-(*R,R*)-1,2-diaminocyclohexane
DN	donor number
ESI-MS	electrospray ionization mass spectrometry
SalbutOH	1,4-bis(salicylideneamino)butan-2-ol
Salen	1,2-bis(salicylidenamino)ethane
Salpn	1,3-bis(salicylidenamino)propane
SalpnOH	1,3-bis(salicylidenamino)propan-2-ol
IC_{50}	concentration for 50% inhibition
LMCT	ligand-to metal charge transfer
NBT	nitro blue tetrazolium
ROS	reactive oxygen species
Salophen	*N,N′*-bis(salicyliden)-1,2-phenylendiamine
SCE	saturated calomel electrode
SOD	superoxide dismutase
TON	total mmol H_2O_2/mmol catalyst

Acknowledgments

We thank the National University of Rosario (BIO401) and CONICET for financial support (PIP 0335) and CONICET-CNRS for a bilateral agreement (Res. 991/2013).

Appendix A. Supplementary data

Crystallographic data for the structures reported in this paper have been deposited with the Cambridge Crystallographic Data Center as Supplementary Publication No. CCDC-1483549 (**1**·H_2O) and CCDC-1483550 (**3**·2DMSO). Supplementary data associated with this article can be found in the online version, at http://dx.doi.org/10.1016/j.jinorgbio.2016.11.019.

References

[1] R.S. Balaban, S. Nemoto, T. Finkel, Cell 120 (2005) 483–495.
[2] F.J. Giordano, J. Clin. Invest. 115 (2005) 500–508.
[3] S. Signorella, C. Palopoli, V. Daier, G. Ledesma, in: R.H. Kretsinger, E.A. Permyakov, V.N. Uversky (Eds.), Encyclopedia of Metalloproteins, Springer, New York 2013, pp. 1283–1292.
[4] W.C. Stallings, K.A. Pattridge, R.A. Strong, M.L. Ludwig, J. Biol. Chem. 260 (1985) 16424–16432.
[5] Y. Sheng, I.A. Abreu, D.E. Cabelli, M.J. Maroney, A.-F. Miller, M. Teixeira, J.S. Valentine, Chem. Rev. 114 (2014) 3854–3918.
[6] V.V. Barynin, M.M. Whittaker, S.V. Antonyuk, V.S. Lamzin, P.M. Harrison, P.J. Artymiuk, J.W. Whittaker, Structure 9 (2001) 725–738.
[7] O. Iranzo, Bioorg. Chem. 39 (2011) 73–87.
[8] S. Signorella, C. Hureau, Coord. Chem. Rev. 256 (2012) 1229–1245.
[9] S.R. Doctrow, K. Huffman, C. Bucay Marcus, G. Tocco, E. Malfroy, C.A. Adinolfi, H. Kruk, K. Baker, N. Lazarowych, J. Mascarenhas, B. Malfroy, J. Med. Chem. 45 (2002) 4549–4558.
[10] M. Baudry, S. Etienne, A. Bruce, M. Palucki, E. Jacobsen, B. Malfroy, Biochem. Biophys. Res. Commun. 192 (1993) 964–968.
[11] Y. Noritake, N. Umezawa, N. Kato, T. Higuchi, Inorg. Chem. 52 (2013) 3653–3662.
[12] D. Moreno, V. Daier, C. Palopoli, J.-P. Tuchagues, S. Signorella, J. Inorg. Biochem. 104 (2010) 496–502.
[13] M.A. Vázquez-Fernández, M.R. Bermejo, M.I. Fernández-García, G. González-Riopedre, M.J. Rodríguez-Doutón, M. Maneiro, J. Inorg. Biochem. 105 (2011) 1538–1547.
[14] V. Daier, D. Moreno, C. Duhayon, J.-P. Tuchagues, S. Signorella, Eur. J. Inorg. Chem. (2010) 965–974.
[15] M. Grau, F. Rigodanza, A.J.P. White, A. Soraru, M. Carraro, M. Bonchio, G.J.P. Britovsek, Chem. Commun. 50 (2014) 4607–4609.
[16] T.P. Ribeiro, C. Fernandes, K.V. Melo, S.S. Ferreira, J.A. Lessa, R.W.A. Franco, G. Schenk, M.D. Pereira, A. Horn Jr., Free Radic. Biol. Med. 80 (2015) 67–76.
[17] A.S. Bernard, C. Giroud, H.Y.V. Ching, A. Meunier, V. Ambike, C. Amatore, M.G. Collignon, F. Lemaître, C. Policar, Dalton Trans. 41 (2012) 6399–6403.
[18] G.N. Ledesma, H. Eury, E. Anxolabéhère-Mallart, C. Hureau, S.R. Signorella, J. Inorg. Biochem. 146 (2015) 69–76.
[19] V.L. Kinnula, J.D. Crapo, Am. J. Respir. Crit. Care Med. 167 (2003) 1600–1619.
[20] B. Day, J. Biochem. Pharmacol. 77 (2009) 285–296.
[21] Y. Rong, S.R. Doctrow, G. Tocco, M. Baudry, Proc. Natl. Acad. Sci. U. S. A. 96 (1999) 9897–9902.
[22] K. Baker, C.B. Marcus, K. Huffman, H. Kruk, B. Malfroy, S.R. Doctrow, J. Pharmacol. Exp. Ther. 284 (1998) 215–221.
[23] Y. Watanabe, A. Namba, N. Umezawa, M. Kawahata, K. Yamaguchi, T. Higuchi, Chem. Commun. (2006) 4958–4960.
[24] E.M. McGarrigle, D.G. Gilheany, Chem. Rev. 105 (2005) 1563–1602.
[25] J.I. Yang, D.G. Nocera, J. Am. Chem. Soc. 129 (2007) 8192–8198.
[26] S.-Y. Liu, J.D. Soper, J.Y. Yang, E.V. Rybak-Akimova, D.G. Nocera, Inorg. Chem. 45 (2006) 7572–7574.
[27] Y.G. Abashkin, S.K. Burt, Inorg. Chem. 44 (2005) 1425–1432.
[28] Y.G. Abashkin, S.K. Burt, J. Phys. Chem. B 108 (2004) 2708–2711.
[29] M. Maneiro, M.R. Bermejo, M.I. Fernández, E. Gómez-Fórneas, A.M. González-Noya, A.M. Tyryshkin, New J. Chem. 27 (2003) 727–733.
[30] E.J. Larson, V.L. Pecoraro, J. Am. Chem. Soc. 113 (1991) 7809–7810.
[31] R. Hage, A. Lienke, J. Mol. Catal. A Chem. 251 (2006) 150–158.
[32] Q.-X. Li, Q.-H. Luo, Y.-Z. Li, Z.-Q. Pan, M.-C. Shen, Eur. J. Inorg. Chem. (2004) 4447–4456.
[33] D. Angelone, S. Abdolahzadeh, J.W. de Boer, W.R. Browne Eur, J. Inorg. Chem. (2015) 3532–3542.
[34] J.A.A.H. Lessa Jr., E.S. Bull, M.R. Rocha, M. Benassi, R.R. Catharino, M.N. Eberlin, A. Casellato, C.J. Noble, G.R. Hanson, G. Schenk, G.C. Silva, O.A.C. Antunes, C. Fernandes, Inorg. Chem. 48 (2009) 4569–4579.
[35] U.P. Singh, P. Tyagi, S. Upreti, Polyhedron 26 (2007) 3625–3632.
[36] M. Maneiro, M.R. Bermejo, M. Fondo, A.M. González, J. Sanmartín, J.C. García-Monteagudo, R.G. Pritchard, A.M. Tyryshkin, Polyhedron 20 (2001) 711–719.
[37] C. Palopoli, B. Chansou, J.P. Tuchagues, S. Signorella, Inorg. Chem. 39 (2000) 1458–1462.
[38] C. Beauchamps, I. Fridovich, Anal. Biochem. 44 (1971) 276–287.
[39] S. Durot, C. Policar, F. Cisnetti, F. Lambert, J.-P. Renault, G. Pelosi, G. Blain, H. Korri-Youssoufi, J.-P. Mahy, Eur. J, Inorg. Chem. 3513–3523 (2005).
[40] Z.R. Liao, X.F. Zheng, B.S. Luo, L.R. Shen, D.F. Li, H.L. Liu, W. Zhao, Polyhedron 20 (2001) 2813–2821.
[41] A. Altomare, G. Cascarano, C. Giacovazzo, A. Guagliardi, SIR-92, J. Appl. Crystallogr. 26 (1993) 343–350.
[42] G.M. Sheldrick, Acta Cryst A64 (2008) 112–122.
[43] M. Maneiro, M.R. Bermejo, A. Sousa, M. Fondo, A.M. González, A. Sousa-Pedrades, C.A. McAuliffe, Polyhedron 19 (2000) 47–54.
[44] J.W. Gohdes, W.H. Armstrong, Inorg. Chem. 31 (1992) 368–373.
[45] H. Shyu, H. Wei, Y. Wang, Inorg. Chim. Acta 290 (1999) 8–13.
[46] L. Sabater, C. Hureau, R. Guillot, A. Aukauloo, Inorg. Chem. 45 (2006) 2373–2375.
[47] G. Bhargavi, M.V. Rajasekharan, J.-P. Costes, J.-P. Tuchagues, Dalton Trans. 42 (2013) 8113–8123.
[48] M.R. Bermejo, A. Garcia-Deibe, J. Sanmartin, A. Sousa, N. Aurangzeb, C.E. Hulme, C.A. McAuliffe, R.G.P. Watkinson, M. Watkinson, Chem. Commun. (1994) 645–646.
[49] M.R. Bermejo, M.I. Fernández, A.M. González-Noya, M. Maneiro, R. Pedrido, M.J. Rodríguez, J.C. García-Monteagudo, B. Donnadieu, J. Inorg. Biochem. 100 (2006) 1470–1478.
[50] M.R. Bermejo, A. Castiñeiras, J.C. Garcia-Monteagudo, M. Rey, A. Sousa, M. Watkinson, C.A. McAuliffe, R.G. Pritchard, R.L. Beddoes, J. Chem. Soc. Dalton Trans. (1996) 2935–2944.
[51] W.J. Geary, Coord. Chem. Rev. 7 (1991) 81–122.
[52] J.A. Bonadies, M.J. Maroney, V.L. Pecoraro, Inorg. Chem. 28 (1989) 2044–2051.
[53] E.J. Larson, V.L. Pecoraro, J. Am. Chem. Soc. 113 (1991) 3810–3818.
[54] M. Hoogenraad, K. Ramkisoensing, W.L. Driessen, H. Kooijman, A.L. Spek, E. Bouwman, J.G. Haasnoot, J. Reedijk, Inorg. Chim. Acta 320 (2001) 117–126.
[55] M.T. Caudle, P. Riggs-Gelasco, A.K. Gelasco, J.E. Penner-Hahn, V.L. Pecoraro, Inorg. Chem. 35 (1996) 3577–3584.
[56] M.R. Bermejo, A.M. González, M. Fondo, A. García-Deibe, M. Maneiro, J. Sanmartín, O. Hoyos, M. Watkinson, New J. Chem. 24 (2000) 235–241.
[57] M.R. Bermejo, A.M. González-Noya, V. Abad, M.I. Fernández, M. Maneiro, R. Pedrido, M. Vásquez, Eur. J. Inorg. Chem. (2004) 3696–3705.
[58] D.P. Kessissoglou, W.M. Butler, V.L. Pecoraro, Inorg. Chem. 26 (1987) 495–503.

[59] K. Bertoncello, G.D. Fallon, K.S. Murray, E.R.T. Tiekink, Inorg. Chem. 30 (1991) 3562–3568.
[60] D. Pursche, M.U. Triller, C. Slinn, N. Reddig, A. Rompel, B. Krebs, Inorg. Chim. Acta 357 (2004) 1695–1702.
[61] E.J. Larson, P.J. Riggs, J.E. Penner-Hahn, V.L. Pecoraro, J. Chem. Soc. Chem. Commun. (1992) 102–103.
[62] C.P. Horwitz, P.J. Winslow, J.T. Warden, C.A. Lisek, Inorg. Chem. 32 (1993) 82–88.
[63] M.J. Baldwin, N.A. Law, T.L. Stemmler, J.W. Kampf, J.E. Penner-Hahn, V.L. Pecoraro, Inorg. Chem. 38 (1999) 4801–4809.
[64] N. Aurangzeb, C.A. McAuliffe, R.G. Pritchard, M. Watkinson, M.R. Bermejo, A. Garcia-Deibe, A. Sousa, Acta Cryst C49 (1993) 1945–1947.
[65] C.E. Hulme, M. Watkinson, M. Haynes, R.G. Pritchard, C.A. McAuliffe, N. Jaiboon, B. Beagley, A. Sousa, M.R. Bermejo, M. Fondo, J. Chem. Soc. Dalton Trans. (1997) 1805–1814.
[66] N.A. Law, J.W. Kampf, V.L. Pecoraro, Inorg. Chim. Acta 297 (2000) 252–264.
[67] H. Torayama, T. Nishide, H. Asada, M. Fujiwara, T. Matsushita, Polyhedron 17 (1998) 105–118.
[68] M. Watkinson, M. Fondo, M.R. Bermejo, A. Sousa, C.A. McAuliffe, R.G. Pritchard, N. Jaiboon, N. Aurangzeb, M. Naeem, J. Chem. Soc. Dalton Trans. (1999) 31–42.
[69] M. Kasuno, M. Hayano, M. Fujiwara, T. Matsushita, Polyhedron 28 (2009) 425–430.
[70] G. González-Riopedre, M.I. Fernández-García, E. Gómez-Fórneas, M. Maneiro, Catalysts 3 (2013) 232–246.
[71] S. Michalkiewicz, M. Kaczor, Chem. Anal. 49 (2004) 121–128.
[72] T. Kurahashi, Inorg. Chem. 54 (2015) 8356–8366.
[73] M.J. Baldwin, T.L. Stemmler, P.J. Riggs-Gelasco, M.L. Kirk, J.E. Penner-Hahn, V.L. Pecoraro, J. Am. Chem. Soc. 116 (1994) 11349–11356.
[74] S. Biswas, K. Mitra, B. Adhikary, C.R. Lucas, Transit. Met. Chem. 30 (2005) 586–592.
[75] C. Hureau, G. Blondin, M.-F. Charlot, C. Philouze, M. Nierlich, M. Césario, E. Anxolabéhère-Mallart, Inorg. Chem. 44 (2005) 3669–3683.
[76] J. Bian, Y. Wang Wei, J. Tang, F.-P. Huang, D. Yao, Q. Yu, H. Liang, Polyhedron 90 (2015) 147–153.
[77] G.B. Shul'pin, G.V. Nizova, Y.N. Kozlov, I.G. Pechenkina, N. J. Chem. 26 (2002) 1238–1245.